Magnon gap formation and charge density wave effect on thermoelectric properties in the $SmNiC_2$ compound

Jin Hee Kim,[1] Jong-Soo Rhyee,[1,*] and Yong Seung Kwon[2,†]

[1]*Department of Applied Physics, Kyung Hee University, Yongin 446-701, Korea*

[2]*Department of Emerging Materials Science, Daegu Gyeongbuk Institute of Science and Technology (DGIST), Daegu 711-873, Korea*

(Received 20 June 2012; published 3 December 2012)

We studied the electrical, thermal, and thermoelectric properties of the polycrystalline compound of $SmNiC_2$. The electrical resistivity and magnetization measurement show the interplay between the charge density wave at $T_{CDW} = 150$ K and the ferromagnetic ordering of $T_c = 18$ K. Below the ferromagnetic transition temperature, we observed the magnon gap formation of $\Delta \simeq 4.3$–4.4 meV by $\rho(T)$ and $C_p(T)$ measurements. The charge density wave is attributed to the increase of the Seebeck coefficient resulting in the increase of the power factor $S^2\sigma$. The thermal conductivity anomalously increases with increasing temperature along the whole measured temperature range, which implies the weak attribution of Umklapp phonon scattering. The thermoelectric figure of merit ZT significantly increases due to the increase of the power factor at $T_{CDW} = 150$ K. Here we argue that the competing interaction between electron-phonon and electron-magnon couplings exhibits the unconventional behavior of electrical and thermal properties.

DOI: 10.1103/PhysRevB.86.235101 PACS number(s): 71.45.Lr, 72.15.Jf, 72.20.Pa, 65.40.−b

I. INTRODUCTION

There has been growing attention given to thermoelectric materials because of the raised awareness of environmentally friendly solid-state cooling and energy harvesting technologies.[1,2] The thermoelectric materials' performance is evaluated by the materials' dimensionless figure of merit ($ZT = S^2\sigma T/\kappa$), where S, σ, T, and κ are the Seebeck coefficient, electrical conductivity, absolute temperature, and thermal conductivity, respectively. Many attempts have been made to increase ZT by employing nanocomposite,[3,4] quantum well, and quantum dot superlattice structures,[5,6] which is based upon the low-dimensional electronic states.[7]

Recently, we proposed that the charge density wave is a promising pathway to enhance ZT by lowering thermal conductivity originated from phonon softening and lattice distortion and by increasing the Seebeck coefficient due to reduced dimensionality of the electronic transport properties.[8–10] In addition, there are many studies on thermoelectric properties in strongly correlated system. For example, the Kondo impurity and Kondo lattice system give rise to the large Kondo resonant peak in the electronic density of states due to the localized f electrons, resulting in the large Seebeck coefficient.[11]

$SmNiC_2$ is a good candidate to investigate the thermoelectric properties of correlated electron behavior. It exhibits the interplay between ferromagnetic ordering at $T_c = 17.7$ K and the charge density wave (CDW) instability at $T_{CDW} = 148$ K, which is a moderately high transition temperature.[12,13] The CDW transition temperatures of $CeTe_2$ and $In_4Se_{3-\delta}$ are quite high near the melting temperatures.[8,9] The intermediate CDW transition temperature of $SmNiC_2$ is appropriate to investigate the effect of CDW on thermoelectric properties. The phonon softening by diffuse x-ray scattering, incommensurate modulation nesting vector of $\mathbf{q} = (0.5, 0.52, 0)$, and peak of the real and imaginary part of the electronic susceptibility at $\mathbf{q} = (0.5, 0.57, 0)$ indicate the two-dimensional charge density wave formation on this compound.[12,14] The x-ray diffraction of $SmNiC_2$ reveals the commensurate CDW state centered on the Ni chain along the **a** direction and the frustrated incommensurate three-dimensional coupling resulting in the incommensurate modulation of the CDW state.[13] From the high-resolution photoemission spectroscopy study, the pseudogap of $\Delta_{PG} \simeq 60$–70 meV gradually appears with lowering the temperature due to the imperfect nature of the Fermi surface nesting.[15] The frustrated interchain coupling and pseudogap state imply the quasi-two-dimensional nature of the charge density wave in $SmNiC_2$.

Here we report the thermoelectric properties of $SmNiC_2$ in terms of electrical resistivity, Seebeck coefficient, heat capacity, and thermal-conductivity measurements. The power factor ($S^2\sigma$) is significantly enhanced by the increase of the Seebeck coefficient in spite of the corresponding increase of electrical resistivity. At low temperatures, we observed the magnon gap opening below the ferromagnetic ordering temperature.

II. EXPERIMENTAL DETAILS

We synthesized the polycrystalline compound of $SmNiC_2$ by the arc-melting method. Due to the vapor pressure of Sm, the initial stoichiometry of the compound was $Sm_{1.1}NiC_2$. The initial stoichiometric mixture of Sm (99.9%), Ni (99.99%), and C (99.99%) was arc melted under a high-purity argon atmosphere. To increase homogeneity, the specimen was turned over and remelted several times. The compound was sealed in a quartz ampoule under high vacuum followed by heat treatment at 1173 K for ten days.

The x-ray diffraction using 12 kW Cu Kα radiation (Rigaku, Japan) showed the single phase of the sample with a $CeNiC_2$-type orthorhombic crystal structure (space group $Amm2$). The lattice parameters were calculated by the least-square refinement with the POWDER CELL and CELREF programs with $a = 3.707$, $b = 4.529$, and $c = 6.099$ Å, which is close to the reported one.[13,16]

We used the physical property measurement system (Quantum Design, Inc.) to measure the electrical resistivity ρ, Seebeck coefficient S, thermal conductivity κ, heat capacity C_p, and Hall resistivity ρ_{xy}. The temperature-dependent electrical resistivity $\rho(T)$ and Seebeck coefficient $S(T)$ were

simultaneously measured by the four-point probe method from 2 to 300 K. We used the thermal relaxation method to measure the thermal conductivity $\kappa(T)$ and heat capacity $C_p(T)$ at $T \leqslant 300$ K. The isothermal Hall resistivity $\rho_{xy}(H)$ measurement was carried out by five-point contact under magnetic fields ranging from 1 to 5 T in order to minimize and eliminate the longitudinal electrical resistivity ρ_{xx}.

III. RESULTS AND DISCUSSION

A. Magnon gap formation

Figure 1(a) shows the temperature-dependent electrical resistivity $\rho(T)$ of $SmNiC_2$. It shows conventional metallic behavior at $150 \leqslant T \leqslant 300$ K. Below 150 K, the $\rho(T)$ is gradually increased from 0.113 to 0.125 mΩ cm at 150 and 120 K, respectively [10.6% enhancement of $\rho(T)$], which is driven by the formation of the CDW energy gap. At the critical temperature $T_c = 18$ K, a drastic decrease of $\rho(T)$ is revealed due to the ferromagnetic ordering. The residual resistivity ratio [RRR $= \rho(300\,\text{K})/\rho(2\,\text{K})$] is very high (RRR = 63.4), indicating good quality of the sample. The CDW ($T_{\text{CDW}} = 150$ K) and ferromagnetic transition ($T_c = 18$ K) behavior of $\rho(T)$ are similar to the previously reported ones.[12,16,17] The significant drop of electrical resistivity near $T_c = 18$ K is the result of the destruction of the CDW state due to the ordered ferromagnetic metallic state. The $\rho(T)$ behavior at $T_{\text{CDW}} = 150$ K is similar to the metal-semiconductor transition feature of the $NbSe_3$ compound.[18] The anomalous transition behavior is explained by the destruction of a partial fraction of the Fermi surface due to the formation of the charge density wave.[19]

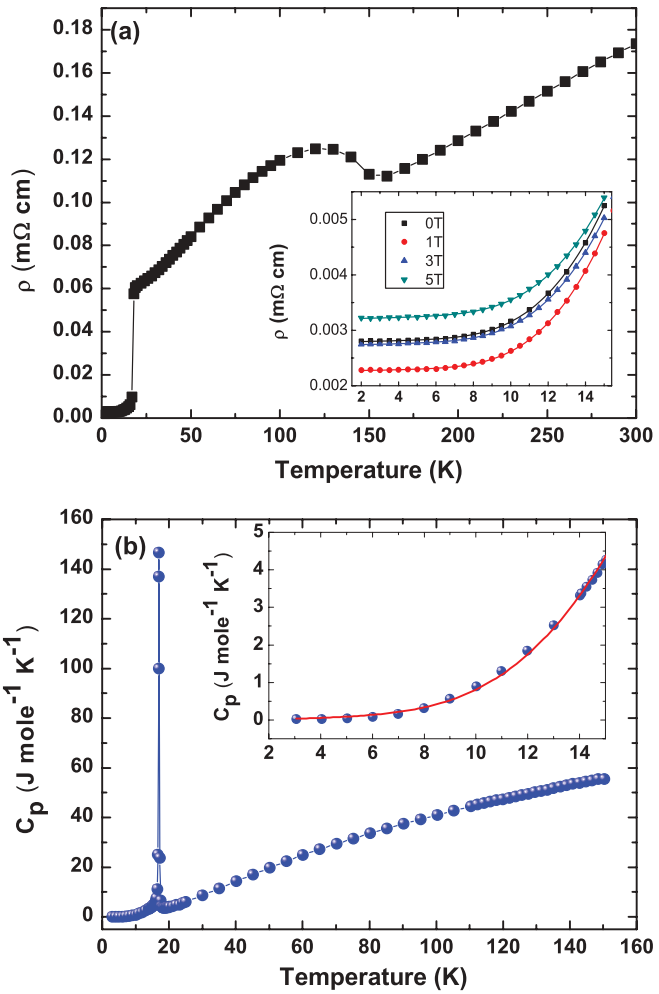

FIG. 1. (Color online) (a) Temperature-dependent electrical resistivity $\rho(T)$ of the $SmNiC_2$ from 2 to 300 K. Inset shows the expanded plot with ferromagnetic magnon gap fitting at low temperatures ($T \leqslant 15$ K) for various magnetic fields of $H = 0$, 1, 3, and 5 T. (b) Temperature-dependent specific heat $C_p(T)$ from 2 to 150 K. Inset shows the expanded plot at low temperatures ($T \leqslant 15$ K) with ferromagnetic magnon gap fitting (red line).

The conventional electrical resistivity should follow T^2-dependent behavior at low temperature in terms of the Fermi-liquid theory. The resistivity fitting to $\rho(T) = \rho_0 + AT^x$ at low temperature ($2 \leqslant T \leqslant 16$ K) gives an unphysical value of $x = 4.8$, where ρ_0 is the residual resistivity and A is the prefactor of metallic resistivity. Instead, the $\rho(T)$ is fitted to the resistivity behavior with Eq. (1), which is associated with the ferromagnetic magnon gap as shown in the inset of Fig. 1(a):[20,21]

$$\rho = \rho_0 + AT^2 + C_m T \Delta\left(1 + 2\frac{T}{\Delta}\right)\exp\left(-\frac{\Delta}{T}\right), \quad (1)$$

where Δ is the magnon gap energy and C_m is the prefactor of resistivity by electron-magnon scattering. The fitted parameters are listed in Table I. The magnon energy gap is slightly increased linearly from 4.37 meV (50.7 K) to 4.42 meV (51.3 K) without and with applying a magnetic field of 5 T, respectively. The explicit form of C_m is

$$C_m = \frac{3\pi}{32} J k_B N_{\text{ion}} A^2 (g_J - 1)^2 \left(\frac{m}{\hbar \epsilon_F^2 e^2}\right), \quad (2)$$

where J is the total angular momentum, N_{ion} is the number of ions per unit volume, A is the interaction between spin and total angular momentum, g_J is the gyromagnetic ratio, and ϵ_F is the Fermi energy. For $J = 5/2$ of Sm^{3+} ($4f^6$), the C_m indicates the ratio between the $\vec{s} \cdot \vec{J}$ interaction and the Fermi energy ϵ_F. If we assume that the $\vec{s} \cdot \vec{J}$ interaction is constant, then the Fermi energy slightly increases by applying magnetic fields because C_m decreases at high magnetic fields ($H \geqslant 1$ T).

The specific heat can measure the magnon contribution at low temperatures. Figure 1(b) shows the temperature dependence of specific heat. The specific heat, including the magnon contribution, can be expressed as $C_p = C_{\text{el}} + C_{\text{ph}} + C_{\text{mag}}$, where the first, second, and third terms represent the electronic, phonon, and magnon contribution, respectively. In the ferromagnetic metal of a noncubic crystal structure, the

TABLE I. The parameters of the fitting result by Eq. (1) from 2 to 16 K under $H = 0$–5 T.

H	ρ_0 ($\mu\Omega$ cm)	A (nΩ cm/K^2)	C_m (nΩ cm/K^2)	Δ (K)
0 T	2.8	1.3	52	50.7
1 T	2.2	1.1	55	51.1
3 T	2.7	1.3	50	51.2
5 T	3.2	1.4	47	51.3

specific heat below T_C can be formulated as

$$C_p = \gamma T + \beta T^3 + \alpha T^{3/2} e^{-\Delta/T}, \quad (3)$$

where α, β, and γ are constants.[20–22] The specific-heat prefactors α, β, and γ below T_C [inset of Fig. 1(b)] are obtained as $\gamma \simeq 8.0$ mJ mol^{-1} K^{-2}, $\beta \simeq 0.4$ mJ mol^{-1} K^{-4}, $\alpha \simeq 6.2$ J mol^{-1} K$^{-2.5}$, and $\Delta \sim 51.8$ K. The magnon gap (Δ) from the specific heat is comparable to the value from the electrical resistivity, which is the evidence of the existence of magnon excitation.

The specific heat shows the anomalously huge value (146.6 J mol^{-1} K^{-1}) and narrow peak (half width at full maximum, HWFM = 0.36 K) near the ferromagnetic transition temperature. This peak value of specific heat at T_c is similar to the ferromagnetic $CeIn_2$ compound.[23] This sharp and narrow peak indicates the first-order magnetic phase transition. The huge value of specific heat is attributed to the significant magnetic contribution of specific heat on this material. When we extract the electronic and phonon contribution of specific heat, the magnetic specific heat at T_c is obtained as $C_m =$ 145.5 J mol^{-1} K^{-1}. It means that the sharp peak of specific heat is mainly from the first-order magnetic phase transition and the huge contribution of magnetic specific heat near the ferromagnetic transition temperature.

Figure 2(a) shows the Hall resistivity ρ_{xy} of $SmNiC_2$ under magnetic field from 1 to 5 T. It shows a conventional linear

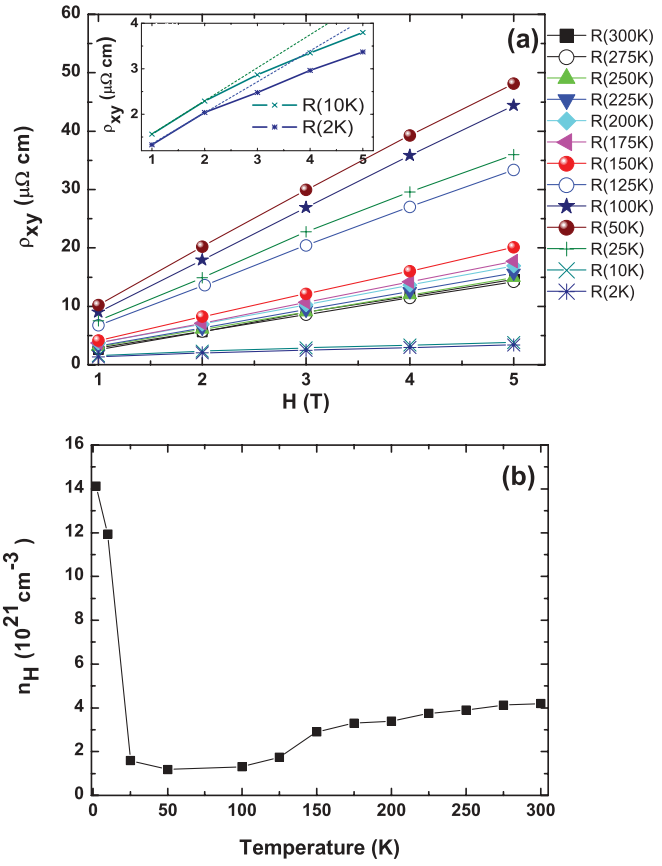

FIG. 2. (Color online) (a) Isothermal field-dependent Hall resistivity $\rho_{xy}(H)$ of the $SmNiC_2$. Inset shows the nonlinear behavior of $\rho_{xy}(H)$ at low temperatures ($T = 2$ and 10 K). (b) Temperature-dependent carrier concentration of $SmNiC_2$.

increase of $\rho_{xy}(H)$ with increasing magnetic fields at high temperatures from 25 to 300 K. At low temperatures ($T \leqslant$ 10 K), we can observe the small nonlinear behavior of ρ_{xy}, as shown in the inset of Fig. 2(a). The nonlinear behavior of $\rho_{xy}(H)$ can be understood by the anomalous Hall effect. In a magnetized material, the Hall resistivity is expressed by $\rho_{xy} = R_0 B + \mu_0 R_1 M$, where R_0 is the ordinary Hall coefficient, B is the magnetic induction, μ_0 is the magnetic permeability of free space, R_1 is the anomalous Hall coefficient, and M is the magnetization.[24] The nonlinear behavior of ρ_{xy} is originated from the skew scattering and side jump effect of the electric charge carrier by magnetic spin due to the ferromagnetic ordering at low temperatures.[25]

When we estimate the Hall carrier concentration by $n_H = 1/(R_0 e)$, where R_0 is the normal Hall coefficient, the Hall carrier density at room temperature is about 4.2×10^{21} cm^{-3}, as shown in Fig. 2(b). The temperature-dependent Hall carrier density decreases linearly with decreasing temperatures from 300 to 150 K. The slope $dn_H(T)/dT$ changes near 150 K, which is caused by the charge density wave gap formation. The reduction of n_H near the CDW transition temperature is consistent with the increase of electrical resistivity at the temperature range. At low temperature ($T \leqslant 20$ K), the carrier density significantly increases with the increase of one order of magnitude. The abrupt metallization is related to the ferromagnetic ordering at $T_c = 18$ K. The ferromagnetic ordering has a destructive effect on the charge density wave, resulting in the emergence of metallization. The abrupt decrease of $\rho(T)$ and the increase of $n_H(T)$ below the ferromagnetic transition temperature were also observed in the EuB_6.[26] In EuB_6, the ferromagnetic ordering competes with a magnetic polaron,[27] whereas in $SmNiC_2$ it competes with the charge density wave instability.

B. Thermoelectric properties

The temperature dependence of Seebeck coefficient $S(T)$ is shown in Fig. 3(a). The positive Seebeck coefficient indicates the holelike charge-carrier transport. The $S(T)$ increases at the CDW transition temperature (150 K), following the broad hump at 110 K ($S = 7.02$ μV/K). The increase of S at the CDW transition temperature is due to the opening of the CDW energy gap. It is well known that the Seebeck coefficient is proportional to the size of the energy gap. The CDW energy-gap opening induces the increase of electrical resistivity and the Seebeck coefficient at the transition temperature. The ratio of increase in the Seebeck coefficient with the S of the CDW onset temperature is $S(110\text{ K})/S(150\text{ K}) = 1.56$; on the other hand, the ratio of increase in electrical resistivity is $\rho(120\text{ K})/\rho(150\text{ K}) = 1.12$. In a simple band picture, there is a trade-off relationship between the Seebeck coefficient and electrical conductivity. In this CDW system, the increase of the Seebeck coefficient is more significant than that of the electrical resistivity.

For metals and degenerate semiconductors, the Seebeck coefficient is expressed by[28]

$$S = \frac{8m^*}{3e}\left(\frac{\pi k_B}{h}\right)^2\left(\frac{\pi}{3n}\right)^{\frac{2}{3}} T, \quad (4)$$

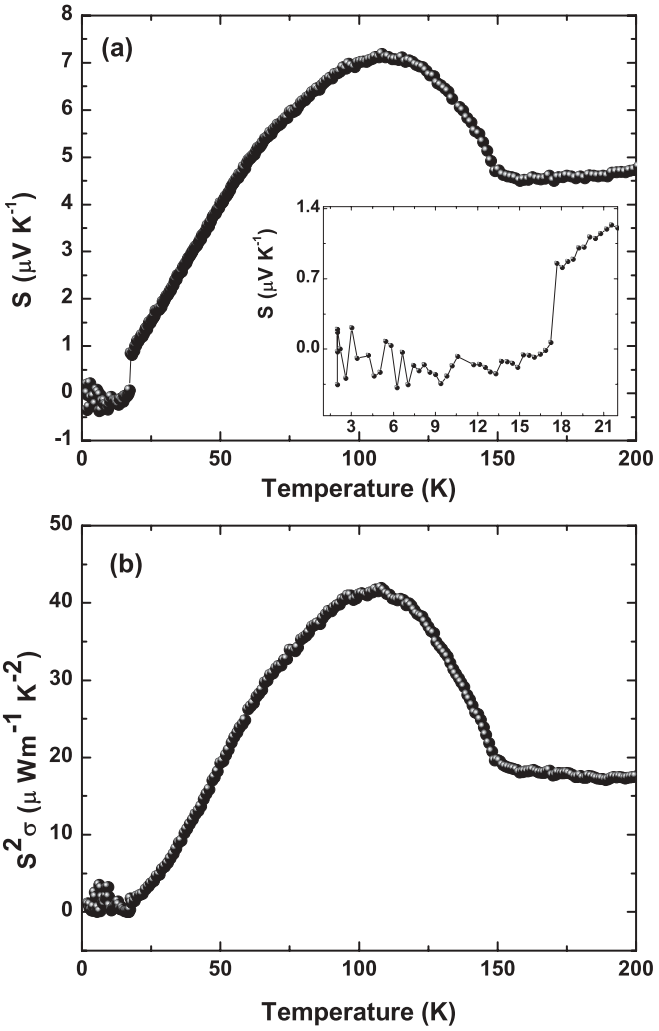

FIG. 3. (a) Temperature-dependent Seebeck coefficient $S(T)$ of the $SmNiC_2$ from 2 to 200 K. Inset shows the expanded plot at low temperatures ($T \leqslant 18$ K). (b) Temperature-dependent power factor (S^2/ρ) of $SmNiC_2$.

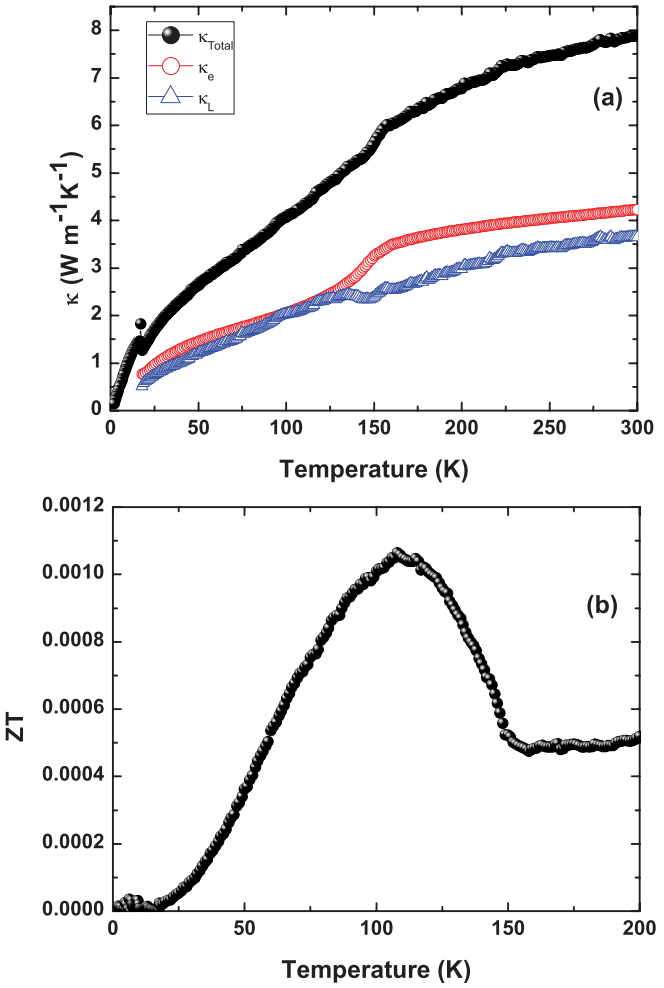

FIG. 4. (Color online) (a) Temperature-dependent total thermal conductivity κ_{tot} (black dot), lattice thermal conductivity κ_L (blue triangle), and electrical thermal conductivity κ_{el} (red circle) of $SmNiC_2$ from 2 to 300 K, calculated from the Wiedemann-Franz law (see text). (b) Temperature-dependent thermoelectric figure of merit (ZT) of $SmNiC_2$ from 2 to 200 K.

where m^*, k_B, h, and n are the effective mass of the carrier, Boltzmann constant, Planck constant, and carrier density, respectively. Using the above equation and the carrier concentration, the increase of effective mass at 100 K m^*(100 K) compared with that of the CDW transition temperature m^*(150 K) is about $m^*(100\text{ K})/m^*(150\text{ K}) = 1.31$; in other words, the effective mass of the charge carrier is increased by the CDW formation. Near the ferromagnetic transition temperatures ($T_c \simeq 17.5$ K), the Seebeck coefficient abruptly decreases to an extremely low value. The significant metallization by the magnetic ordering results in the electron and hole mixing, which gives rise to the low Seebeck coefficient.

Owing to the increase of the Seebeck coefficient, the power factor S^2/ρ is increased at the CDW transition temperature, as shown in Fig. 3(b). The maximum value of the power factor is relatively small, 41.93 μW m^{-1} K^{-2}, at 108 K compared with values of the conventional thermoelectric materials, such as Bi_2Te_3.[29] However, it definitely shows that the thermoelectric performance is increased by the CDW gap formation in $SmNiC_2$, as we reported that the CDW gap can optimize the power factor.[8] From the high-resolution photoemission spectroscopy, the CDW energy gap of $SmNiC_2$ is revealed as the partial pseudogap of $\Delta_{PG} \simeq 60$–70 meV.[15] This energy gap is very small to have a high thermoelectric performance.[30] The larger CDW energy gap may give rise to the larger power factor on this material. At low temperature, the competing behavior with the ferromagnetic ordering suppresses the CDW energy gap, resulting in the decrease of the power factor.

The temperature-dependent thermal conductivity is shown in Fig. 4(a). The decrease of thermal conductivity near 150 K and sharp transition near 17 K correspond to the CDW and ferromagnetic phase transitions, respectively. The total thermal conductivity is increased with the increasing temperature. At room temperature, the total thermal conductivity is about 7.9 W m^{-1} K^{-1}. The total thermal conductivity composes with the electric and phonon contribution of thermal conductivity, $\kappa_{total} = \kappa_{el} + \kappa_{ph}$, where κ_{el} and κ_{ph} are the electronic and phonon thermal conductivity, respectively. The electronic thermal conductivity is calculated by the Wiedemann-Franz law, $\kappa_{el} = L_0\sigma T$, where L_0 is the Lorenz number $L_0 =$

2.45×10^{-8} WΩ/K^2. The electronic thermal conductivity is 4.2 W m^{-1} K^{-1}, and the lattice thermal conductivity is 3.7 W m^{-1} K^{-1} at room temperature. Interestingly, the lattice thermal conductivity obtained by the subtraction of electronic thermal conductivity exhibits a linear increase behavior with increasing temperature. This is very unusual behavior because, in conventional materials, the lattice thermal conductivity exhibits a $1/T$-type decrease of thermal conductivity at high temperature ($T \geqslant \Theta_D$) due to the Umklapp phonon-scattering process of the acoustic phonon. At sufficiently low temperature, the freezing of Umklapp scattering decreases the lattice thermal conductivity, which shows the maximum value near the freezing temperature and follows the exponential decrease of thermal conductivity $e^{T_0/T}$ with decreasing temperature, where T_0 is the temperature of the order of Debye temperature Θ_D.[31] We cannot observe the $1/T$-type acoustic phonon contribution of lattice thermal conductivity as well as the freezing out of the Umklapp scattering in the lattice thermal conductivity.

The increase of thermal conductivity at high temperature is also observed in the CDW compound of $Lu_5Ir_4Si_{10}$.[32] The CDW melting was investigated on this material by time-resolved pump-probe reflectivity measurement and spectral weight analysis.[33] The compound exhibits the freezing out of Umklapp scattering and $1/T$ temperature dependence of thermal conductivity at low temperature ($T \leqslant 90$ K). However, the anomalous increase of $\kappa(T)$ at high temperature was not resolved well. We can consider two possible reasons for this unusual behavior of thermal conductivity on the $SmNiC_2$ compound. First, the Wiedemann-Franz law is based upon the relaxation-time approximation with constant relaxation time. When we take into account the impurity scattering, electron-phonon interaction, and electron-hole bipolar diffusion, the electric thermal conductivity is not simply described by the Wiedemann-Franz law. In the $SmNiC_2$ compound, the competing interaction between ferromagnetic ordering and the charge density wave with strong electron-phonon coupling complicates the electrical thermal conductivity. This is reasonable because the lattice thermal conductivity, obtained by the subtraction of the electrical conductivity from total thermal conductivity, $\kappa_{ph} = \kappa_{tot} - \kappa_{el}$, is negative below the ferromagnetic transition temperature, which indicates violation of the Wiedemann-Franz law. Second, the quasiparticle scattering of the acoustic phonon with the fluctuation effect in the charge density wave can increase thermal conductivity.[32] The increase of thermal conductivity with increasing temperature is widely observed in the disordered or guest-free rattling compounds.[34] The disordered phonon scattering exhibits the unconventional behavior of thermal conductivity with temperature. The fluctuation effect of CDW on the $SmNiC_2$ compound may give rise to the increase of lattice thermal conductivity. More intensive investigations are needed using single-crystalline materials to understand the anomalous temperature-dependent behavior of thermal conductivity.

Figure 4(b) shows the temperature-dependent dimensionless figure of merit (ZT). Owing to the increase of the power factor below the CDW transition, the ZT value is increased at the temperature range. The maximum ZT_{max} value is 1.06×10^{-3} at 108 K. In spite of the small value of ZT_{max}, the increase of the power factor and ZT driven by the CDW energy-gap formation indicates that the optimization of the CDW energy gap is an essential ingredient to maximize the ZT value on the CDW materials.

IV. CONCLUSIONS

The coexistence of the charge density wave and ferromagnetic phase transitions at $T_{CDW} = 150$ K and $T_c = 18$ K, respectively, is observed in the $SmNiC_2$ compound. The ferromagnetic transition significantly decreases the electrical resistivity due to the significant increase of electrical carrier density. Below T_c, the magnon gap formation ($\Delta \approx 4.3$–4.4 meV) is observed from the electrical resistivity and heat-capacity measurements. The magnon gap is increased by increasing magnetic fields up to 5 T. The significant metallization from the increase of carrier density below T_c gives rise to the extremely small Seebeck coefficient. The thermal-conductivity measurements show that the Wiedemann-Franz law is violated in a strong electron-phonon and electron-magnon coupling limit. The CDW energy-gap formation at $T_{CDW} = 150$ K increases the Seebeck coefficient and effective mass of carriers, resulting in the increase of the power factor and ZT values. In spite of the low values of ZT_{max}, we showed that the CDW gap formation is a useful way to optimize the ZT value.

ACKNOWLEDGMENTS

J.S.R. was supported by the Basic Science Research Program (Grant No. 2011-0021335), Nano-Material Technology Development Program (Grant No. 2011-0030147), and Basic Science Research Program (Grant No. 2012R1A2A1A03005174) through the National Research Foundation of Korea (NRF) funded by the Ministry of Education, Science and Technology, Energy Efficiency and Resources program of the Korea Institute of Energy Technology Evaluation and Planning (KETEP) grant funded by the Korean government Ministry of Knowledge Economy (Grant No. 20112010100100), and TJ Park Junior Faculty Fellowship funded by the POSCO TJ Park Foundation. Y.S.K. was supported by the Basic Science Research Program (Grant No. 2010-0007487) and the Mid-career Researcher Program (Grant No. 2010-0029136).

*Corresponding author: jsrhyee@khu.ac.kr
†Corresponding author: yskwon@dgist.ac.kr

[1] F. J. DiSalvo, Science **285**, 703 (1999).
[2] J. Yang and T. Caillat, MRS Bull. **31**, 224 (2006).
[3] M. Zebarjadi, G. Joshi, G. Zhu, B. Yu, A. Minnich, Y. Lan, X. Wang, M. Dresselhaus, Z. Ren, and G. Chen, Nano Lett. **11**, 2225 (2011).
[4] B. Poudel, Q. Hao, Y. Ma, Y. Lan, A. Minnich, B. Yu, X. Yan, D. Wang, A. Muto, D. Vashaee, X. Chen, J. Liu, M. S. Dresselhaus, G. Chen, and Z. Ren, Science **320**, 634 (2008).
[5] L. D. Hicks, T. C. Harman, X. Sun, and M. S. Dresselhaus, Phys. Rev. B **53**, R10493 (1996).
[6] T. C. Harman, P. J. Taylor, M. P. Walsh, and B. E. LaForge, Science **297**, 2229 (2002).

[7]M. S. Dresselhaus, G. Chen, M. Y. Tang, R. Yang, H. Lee, D. Wang, Z. Ren, J.-P. Fleurial, and P. Gogna, Adv. Mater. **19**, 1043 (2007).
[8]J.-S. Rhyee, E. Cho, K. H. Lee, S. I. Kim, E. S. Lee, S. M. Lee, and Y. S. Kwon, J. Appl. Phys. **105**, 053712 (2009).
[9]J.-S. Rhyee, K. H. Lee, S. M. Lee, E. Cho, S. I. Kim, E. Lee, Y. S. Kwon, J. H. Shim, and G. Kotliar, Nature (London) **459**, 965 (2009).
[10]J.-S. Rhyee, E. Cho, K. H. Lee, S. M. Lee, S. I. Kim, H.-S. Kim, Y. S. Kwon, and S. J. Kim, Appl. Phys. Lett. **95**, 212106 (2009).
[11]S. Paschen, *Thermoelectrics Handbook: Macro to Nano*, (CRC/Taylor & Francis, New York, 2006), Chap. 15.
[12]S. Shimomura, C. Hayashi, G. Asaka, N. Wakabayashi, M. Mizumaki, and H. Onodera, Phys. Rev. Lett. **102**, 076404 (2009).
[13]A. Wölfel, L. Li, S. Shimomura, H. Onodera, and S. vanSmaalen, Phys. Rev. B **82**, 054120 (2010).
[14]J. Laverock, T. D. Haynes, C. Utfeld, and S. B. Dugdale, Phys. Rev. B **80**, 125111 (2009).
[15]T. Sato, S. Souma, K. Nakayama, T. Takahashi, S. Shimomura, and H. Onodera, J. Phys. Soc. Jpn. **79**, 044707 (2010).
[16]H. Onodera, Y. Koshikawa, M. Kosaka, M. Ohashi, H. Yamauchi, and Y. Yamaguchi, J. Magn. Magn. Mater. **182**, 161 (1998).
[17]M. Murase, A. Tobo, H. Onodera, Y. Hirano, T. Hosaka, S. Shimomura, and N. Wakabayashi, J. Phys. Soc. Jpn. **73**, 2790 (2004).
[18]G. Grüner, *Density Waves in Solids* (Addison Wesley, Tokyo, 1994), Chap. 3.
[19]N. P. Ong and P. Monceau, Phys. Rev. B **16**, 3443 (1977).
[20]T. Fukuhara, R. Yamagata, L. Li, K. Nishimura, and K. Maezawa, J. Phys. Soc. Jpn. **78**, 034723 (2009).
[21]N. Hessel Andersen and H. Smith, Phys. Rev. B **19**, 384 (1979).
[22]O. V. Lounasmaa and L. J. Sundström, Phys. Rev. **150**, 399 (1966).
[23]D. P. Rojas, J. I. Espeso, J. Rodríguez Fernández, and J. C. Gómez Sal, Phys. Rev. **80**, 184413 (2009).
[24]R. Karplus and J. M. Luttinger, Phys. Rev. **95**, 1154 (1954)
[25]C. L. Chen, *The Hall Effect and Its Applications* (Plenum, New York, 1979).
[26]S. Süllow, I. Prasad, M. C. Aronson, J. L. Sarrao, Z. Fisk, D. Hristova, A. H. Lacerda, M. F. Hundley, A. Vigliante, and D. Gibbs, Phys. Rev. B **57**, 5860 (1998).
[27]Unjong Yu and B. I. Min, Phys. Rev. Lett. **94**, 117202 (2005).
[28]G. J. Snyder and E. Toberer, Nature Mater. **7**, 105 (2008).
[29]X. Ji, J. He, Z. Su, N. Gothard, and T. M. Tritt, J. Appl. Phys. **104**, 034907 (2008)
[30]J. O. Sofo and G. D. Mahan, Phys. Rev. B **49**, 4565 (1994).
[31]N. W. Ashcroft and N. D. Mermin, *Solid State Physics* (Saunders College Publishing, Orlando, 1976), Chap. 25.
[32]Y. K. Kuo, C. S. Lue, F. H. Hsu, H. H. Li, and H. D. Yang, Phys. Rev. B **64**, 125124 (2001).
[33]B. Mansart, M. J. G. Cottet, T. J. Penfold, S. B. Dugdale, R. Tediosi, M. Chergui, and F. Carbone, Proc. Natl. Acad. Sci. **109**, 5603 (2012).
[34]G. S. Nolas, J. Yang, and H. J. Goldsmid, *Thermal Conductivity: Theory, Properties, and Applications*, edited by T. M. Tritt, (Springer, New York, 2004), Chap. 1.5.